Enhancing land use: Integrating bifacial PV and olive trees in agrivoltaic systems

Elmehdi Mouhib [a,*], Álvaro Fernández-Solas [a], Pedro J. Pérez-Higueras [a], Ana M. Fernández-Ocaña [b], Leonardo Micheli [c], Florencia Almonacid [a], Eduardo F. Fernández [a]

[a] *Advances in Photovoltaic Technology (AdPVTech), CEACTEMA, University of Jaén (UJA), 23071 Jaén, Spain.*
[b] *Departamento de Biología Animal, Biología Vegetal y Ecología, Facultad de Ciencias Experimentales, University of Jaén, Las Lagunillas Campus, Jaén 23071, Spain*
[c] *Department of Astronautical, Electrical and Energy Engineering (DIAEE), Sapienza University of Rome, 00184 Rome, Italy*

HIGHLIGHTS

- An agrivoltaic system of bifacial PV and three varieties of olive trees were studied.
- The raytracing approach and olive light response were used to model the tree yield.
- The influences of photovoltaic module height and tilt were quantified.
- The peak land equivalent ratio (LER) of 71% resulted when PV panels were tilted at 20°.
- The study revealed that olive trees displayed moderate sensitivity to shading.

ARTICLE INFO

ABSTRACT

Agrivoltaic systems provide a promising solution for mitigating the competition for land between food and energy production. This study examines the performance of an agrivoltaic system in southern Spain, which integrates bifacial PV technology with three different olive cultivars. Different configurations of clearance height and PV modules tilt are analyzed. The findings indicate that PV modules tilted near the site's latitude achieve the highest energy yield, while vertically-oriented modules lead to the greatest olive yield. The variation in tilt angle has a more significant impact on PV yield, whereas the height of the PV modules primarily affects olive tree yield. To quantify the combined land productivity of energy and crop outputs, the land equivalent ratio (LER) is employed. The results demonstrated a maximum LER of 171% when modules are tilted at 20°, thereby enhancing overall land productivity. Moreover, the study reveals that olive trees display a moderate sensitivity to shading. These findings underscore the importance of optimizing the configuration of PV systems for dual land use in agrivoltaic while taking agricultural productivity into account.

1. Introduction

The global consumption of food has been on a rapid rise, reaching a staggering 2.5 billion metric tons in 2021 [1]. This significant increase has created a growing demand for agricultural land to meet the food production requirements. However, the simultaneous growth in the world's population has led to a surge in energy consumption. While photovoltaic (PV) technology offers many positive aspects to address this energy demand, it also presents a challenge in terms of land use conflict with agriculture, necessitating a tradeoff between food and energy production. In this context, agrivoltaic (APV) systems emerge as a promising solution by leveraging the dual use of land. These innovative systems facilitate crop cultivation for food production while harnessing solar energy. APV systems are classified based on several factors, including the system type (closed or open) and the structure type (interspace PV, overhead PV, PV-integrated greenhouses) [2].

The dual food-energy production is not the only advantage of APV systems, as they also contribute reducing the irrigation water budget [3] and retaining the soil moisture during the summers. Depending of the shade level, the water saving can be as high as 29% [4]. Also the temperature under the panel is moderated [5]. In addition, APV systems can

---

* Corresponding author at: Building A3, Office 452 Campus Las Lagunillas, s/n, 23071 Jaén, Spain.
E-mail address: emouhib@ujaen.es (E. Mouhib).

Nomenclature

Symbols

P_{PV}	PV power per unit active area, W/m^2
G_{front}	Front irradiance on the PV module, W/m^2
G_{rear}	Rear irradiance on the PV module, W/m^2
G_{eff}	Effective irradiance, W/m^2
η_{STC}	PV module efficiency under Standard Test Conditions, unitless
φ	Bifaciality factor, unitless
SF_{front}	Front spectral factor, unitless
SF_{rear}	Rear spectral factor, unitless
SR_{front}	Front spectral response, A/W
SR_{rear}	Rear spectral response, A/W
$E_{front,ref}$	Front reference spectra, W/(m^2.nm)
$E_{rear,ref}$	Rear reference spectra, W/(m^2.nm)
G_{front}	Front broadband global irradiance, W/m^2
G_{rear}	Rear broadband global irradiance, W/m^2
$G_{front,ref}$	Front broadband reference irradiance, W/m^2
$G_{rear,ref}$	Rear broadband reference irradiance, W/m^2
T_{cell}	PV cell temperature, °C
$T_{cell,STC}$	PV cell temperature under STC, °C
T_a	Ambient temperature, °C
E_{plant}	Incident spectrum of the plant, W/(m^2.nm)
G	Global broadband irradiance on the olive tree, W/m^2
GHI	Spectral global irradiance, W/(m^2.nm)
$PPFD_{plant}$	Photosynthetic photon flux density, μmol/(m^2•s)
$PPFD$	Corrected photosynthetic photon flux density, μmol/(m^2•s)
N_A	Avogadro's number mol^{-1}
h	Planck's constant m^2 kg / s
c	Light velocity, m/s
F_0	Minimal fluorescence, dark-adapted conditions, a.u.
$F_0^{'}$	Minimal fluorescence, light-adapted conditions, a.u.
F_m	Maximal fluorescence, dark-adapted conditions, a.u.
$F_m^{'}$	Maximal fluorescence, light-adapted conditions, a.u.
E_{Licor}	Spectral distribution of Licor LI-6800 light source, W/(m^2. nm)
$Y_{PV,APV}$	Energy yield for APV system, KWh/m^2
$Y_{PV,ref}$	Energy yield of a reference traditional PV, KWh/m^2
$Y_{crop,APV}$	Olive trees yield, APV system, mol (CO_2)/m^2
$Y_{crop,ref}$	Olive trees yield, the reference open field system, mol (CO_2)/m^2
R_{GR}	Light shading ration, unitless
m	Olive tree sensitivity to shading, unitless
R^2	Coefficient of determination

Abbreviations

LER	Land equivalent ratio, unitless
PV	Photovoltaic
bPV	Bifacial photovoltaic
APV	Agrivoltaics
PAR	Photosynthesis active radiation
PSN	Photosynthetic rate, μmol (CO_2)/(m^2•s)
TMY	Typical meteorological year
BR	Bifacial Radiance
LCOE	Levelized cost of electricity
STC	Standard test conditions
AOIF	Angle of incidence factor, unitless
AOI	Angle of incidence, °
SF	Spectral factor, unitless
BSF	Bifacial spectral factor, unitless
TF	Thermal factor, unitless
MM	Mismatch factor, unitless
c-Si	Crystalline silicon
NOCT	Nominal Operating Cell Temperature
DC/AC	Alternating current & Direct current
QY	Quantum yield
RMSE	Root mean square error
MBE	Mean bias error

produce the energy needed by the irrigation pumping equipment, which is particularly important in locations where there is no electricity grid. In overhead APV systems, PV panel arrays are strategically designed to partially cover crops with an optimal density, elevation, and tilt. These factors are determined based on the desired balance for sunlight distribution between the PV panels and the agricultural area. To achieve this balance, it is crucial to simultaneously assess the crop and PV yields. This assessment helps identify suitable crop types based on the level of shading underneath the panels, as well as determine the optimal configuration of the PV system to maximize energy harvesting.

In APV, the incident light is shared between PV panels and plants. As a consequence, the available light intercepted by the plants for photosynthesis can be reduced. The process of plant photosynthesis is influenced not only by environmental conditions but also by genetic factors. Therefore, it is essential to select plant species that can adapt to lower levels of incident light. One important genetic factor, which can be used to make this selection, is the carbon assimilation pathway. It categorizes plant species into C3, C4, and CAM types [6]. C3 species have a tendency to saturate at low levels of photosynthesis active radiation (PAR) [7]. This means that they are shade-tolerant [8] and, thus, they are suitable for APV systems, as they can grow even under reduced light conditions. By selecting C3 species, the negative impact of shading caused by the PV panels can be mitigated, ensuring that the plants can still conduct efficient photosynthesis in APV systems. Olive trees are C3 species [9] and, for this reason, they represent a promising choice for APV systems. Olive trees are known for their ability to tolerate shade [10], making them

adaptable to the reduced light conditions that can occur under PV modules. In addition, the global olive tree population is exceeding 850 million trees and occupies approximately 8.7 million hectares of land [11], which indicates that a substantial land area is potentially available for APV systems.

There are several approaches available to evaluate the effects of different APV configurations on crops. One option is to conduct simulations that assess crop yield under varying environmental conditions. These simulations take into account the interaction between soil and plants, farming techniques, as well as microclimate parameters [12,13]. A simplified method, which models only the available photosynthetically active radiation under the PV panels [14], has also been used. Another way to evaluate crop productivity is by considering the incident spectral irradiance along with the spectral absorption of the plants [15]. This approach provides the instantaneous photosynthetic rate (PSN), and by integrating the PSN over time, it yields the amount of CO2 absorbed through photosynthesis during a certain time interval. This latter value acts as the main output of the crop model.

The adoption of orchard trees, as olive trees, in APV systems has also been studied in different papers. In [16], apple trees were cultivated under different shading levels in the south of France. The results showed a decrease in the irrigation requirements when orchard trees were incorporated into the APV system. The results also demonstrated that the PV panels provided protection against freezing damage on the trees. However, it was observed that high levels of shading (40%) had negative consequences on the annual yields of the apple trees. Another study

focused on the growth of kiwi fruit under PV panels at different shading levels [17]. The findings indicated that as the shading levels increased, there was a decrease in the PSN attributed to a reduction in solar radiation, and a decrease in the tree's leaf water use efficiency. The case study in [18] focused on Arbequina olive trees in an APV configuration in southern Italy. The objective of the study was to examine the potential for enhancing land utilization through APV systems. By simulating three levels of sensitivity to shading, the authors found that it is feasible to implement APV systems into olive groves. Another study on the potential of agrivoltaic systems within olive groves in the Mediterranean region has assessed the feasibility of integrating photovoltaics into these groves [19]. The study has also identified representative locations where this application is applicable, and Spain is one of them. Our study holds significant novelty and importance in comprehensively evaluating the yields of both photovoltaic systems and olive trees within the context of APV systems. By considering three distinct olive varieties (Picual, Manzanilla, and Chemlali) and exploring various configurations of bifacial PV systems, the research aims to optimize the overall yields of energy generation and olive production. One key aspect is the investigation of the sensitivity of the olive tree varieties to different levels of shading, providing valuable insights into their specific requirements and responses. The findings of this study will contribute to the refinement of the PV system configurations and to the effective integration of PV modules into the olive orchards, thus facilitating the development of APV systems. This research fills a crucial knowledge gap in the field and offers practical implications for maximizing the sustainability and productivity of APV system settings.

This work is structured as follows. Section 2: The approach used for modeling the amount of solar radiation that reaches the trees and PV modules in an APV system with olive trees is described, along with the details of the methodology adopted to determine the PV and olive yields. Section 3: The results are presented, considering different PV configurations and their impact on the performance of both the PV system and olive trees. Additionally, the sensitivity of olive varieties to shading levels is examined. Section 4: The overall conclusions regarding the feasibility of APV systems are provided, along with suggestions for future research to further enhance this study.

2. Material and methods

The approach used in this study is grounded in modeling the amount of solar radiation that reaches the trees and the PV modules in an APV system with olive trees. Then, from the modeled values, both the crop and the PV yields are calculated. The primary objective of this study is to enhance the PV system design in order to optimize its integration into a pre-existing olive field. There are different modes of olive cultivation, such as traditional, intense, and super-intensive approaches [20]. Particularly, this work focuses on super-intensive cultivation. In this type of olive farming, the trees are typically arranged in a rectangular layout with a planting pattern of 4–5 m × 2–3 m [21], thus providing sufficient room between rows to accommodate PV modules. The trees themselves have a relatively low height of 2–3 m [22]. Additionally, super-intensive plantations require moderately sloping soils, which facilitate the installation of PV structures [23]. Despite being utilized on only 3% of the world's olive-growing hectares, this approach provides a remarkable 36% contribution to the total global olive oil production [24], owing to its higher yields. Furthermore, olive groves are widespread, spanning 66 countries and covering an extensive 11.6 million hectares in total, with an 400,000 ha dedicated to super-intensive density cultivation [25]. This super-intensive layout shows promise as it combines olive cultivation with PV energy generation in a space-efficient and practical manner. Indeed, it offers a dual-purpose solution for utilizing the same area effectively. In this study, bifacial PV modules are considered to improve the PV yield by capturing sunlight from the front and the rear sides of the modules [26].

Fig. 1 presents the methodology employed in this study, showcasing the systematic approach used to evaluate and analyze the olive tree and photovoltaic yields across various PV configurations. The simulations have been conducted considering Jaén, Spain (37.77° N, 3.78° W) as location. This selection is motivated by the 2430 km² of land surface covered by olive trees in Jaén province [27]. To obtain the irradiance and temperature values of the site, typical meteorological year (TMY) data were downloaded from PVGIS [28]. These data were utilized in the simulation to account for the meteorological variability of the location. The hourly values of direct and diffuse irradiance were utilized as inputs for the ray-tracing tool "Bifacial Radiance" (BR) [29], which was employed to simulate the radiation that reaches both the olive trees and the PV modules. This tool was specifically designed for modeling the
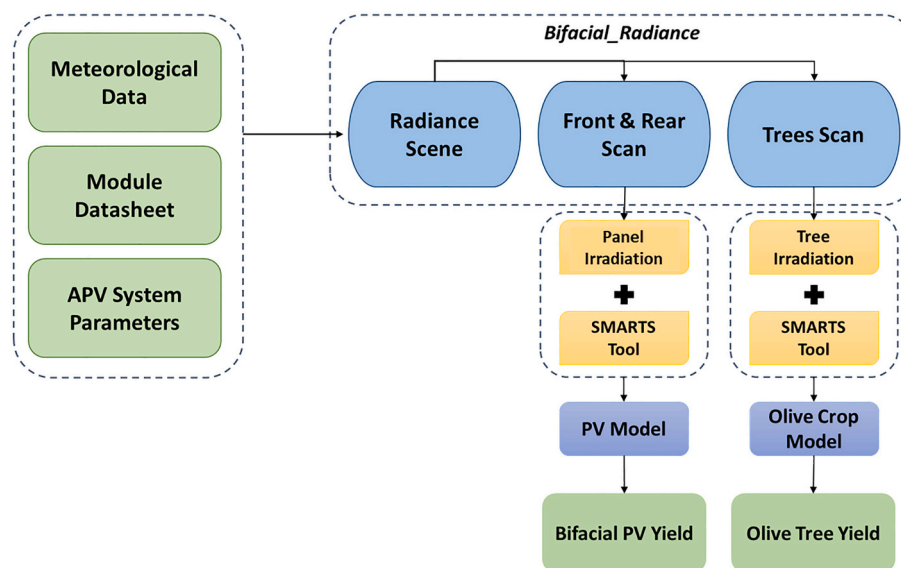

Fig. 1. Schematic of the agrivoltaic system model with bifacial PV modules. The scene includes a field of olive trees along with the PV modules. Then a scan of the scene is performed to calculate the amount of solar radiation captured by both the front and rear sides of the bifacial PV modules, as well as that captured by the olive trees.

3

performance of bifacial PV modules and has been used in multiple research studies [30–32]. The PV system is characterized by the number, size, tilt angle and orientation of the modules that comprise it. On the other hand, the olive grove is represented with the olive trees dimensions, the distances between trees and the distance between rows of trees. In the next subsection, the methodology used to calculate the yield of both the PV system and the olive trees is explained. This provides insights into the factors that influence the performance of the combined APV system.

2.1. Irradiance simulation

In the configuration known as "interspace APV", the modules can be installed using the available space between tree rows. This particular type of APV system is well-suited for super-intensive cultivation because of its row spacing of approximately 3.5 m. This distance between the rows allows ample space for the installation of PV in between. One crucial factor to consider when designing the PV structure is that it should not hinder the normal operation of the harvesting machine. Therefore, the structure must be carefully planned and constructed to allow the harvesting machine to move freely and work efficiently without any impediments. To ensure that the harvesting machines used in olive harvesting can operate freely, the minimum height of the PV system structures considered for this study was 3 m [33,34]. To model the energy yield of the PV system, the hourly TMY data from PVGIS [28] was used as input to the Radiance raytracing simulation tool [29]. To simplify the simulation process, the scene was divided into two parts: (i) the olive trees, which were characterized by the dimensions of the trunk and the crown, and (ii) the PV system. Thus, as shown in Fig. 2, each tree was approximated as two cylindrical shapes, one above the other, with dimensions that reproduce those of real super-intensive olive trees [21]. The trunk has a radius of 0.25 m and a height of 1 m, while the crown has a radius of 1 m and a height of 1.5 m. The total height for the three varieties is therefore considered to be 2.5 m, which represents the average height of olive trees in a super-intensive cultivation approach [35].

The amount of solar radiation that reaches the rear side of the bifacial PV module is directly linked to the albedo coefficients of both the trees and the ground. In this study, the broadband albedo used for trees is 0.309, which is derived from the spectral albedo data of the Picual variety obtained from [36]. An assumption has been made to consider the same albedo for all three varieties due to the lack of alternative reflectance data available in the literature. Also, the light soil was used as ground albedo with a broadband albedo of 0.25.

The second part of the scene is the PV system, which is defined with PV modules tilt angle and the orientation to optimize the energy production. In order to determine an appropriate size for the APV system, a sensitivity analysis was conducted by considering different numbers of tree rows (from 8 to 18). The objective was to determine whether increasing the number of rows beyond 8 would have any significant impact on the amount of solar irradiance received by a central tree. The findings indicated that the increase in the APV field size considered in the simulation did not result in any discernible effect on the amount of sunlight received by the trees. On average, the solar irradiance received by a tree in the central row exhibited a 0.27% variation only. Based on these results, it was concluded that an APV configuration comprising 8 rows of trees was appropriate for the study. A bifacial module with dimensions of 1.755 m in height and 1.038 m in width was employed in the simulations [37]. The complete scene is presented in Fig. 2. The farm area remained constant at 860 m^2, which corresponds to a rectangular shape with a length of 41.42 m and a width of 20.76 m. This area accommodates 8 rows of olive trees and 7 rows of bPV modules. To determine the incident irradiance that reaches the trees and the PV modules, multiple sensors were placed on both elements in the Bifacial Radiance scene. Five sensors are placed on the PV module: four sensors are positioned in each corner, and the fifth sensor is placed in the center of the module. PV sensors were positioned on a central PV module within the central PV row. This was done to acquire irradiance values on PV modules simulated without interaction with edge effects. Subsequently, the average irradiance measured by the sensors was calculated. For the trees, four sensors per tree were employed, as shown in Fig. 2. The positioning of the tree sensors was specifically chosen to measure the irradiance at various points on the tree crown, namely E (east), W (west), S (south), and N (north). The results of the simulation were then used as inputs to the PV and olive models, which are detailed in the next section.

The tilt angle and hub height (h) of the PV modules are the adjustable parameters used to optimize both PV and olive yields. However, for all simulations, the orientation was fixed to the south. Although varying the orientation can yield different results for the PV, the south orientation is being considered to maximize annual energy yield [38], particularly in regions with latitude angles exceeding 30° [38]. Nevertheless, optimizing the income of the APV system, while considering fluctuations in energy prices, a different optimum orientation may emerge, potentially resulting in a lower levelized cost of electricity (LCOE). One of the primary reasons for varying the tilt angle and hub height of PV panels, as illustrated in Fig. 3, is to assess the impact of shading levels on olive trees and investigate their sensitivity to radiation intensity. In order to cover all possible angles, the tilt angle of the PV modules was systematically altered from 0 to 90°. While angles as low as 0° may raise practical concerns related to rainfall, our aim was to gain a comprehensive understanding of yield patterns by exploring this extensive spectrum of angles. Similarly, the hub height was varied between 3 m and 4.5 m. Lower heights were not considered to ensure that the harvesting machine could operate under normal conditions. In super-intensive cultivations, a lower height harvesting machine is typically adopted, such as the "ALMONDS'LINE" machine [39], which has a height of 3.3 m and an overall width of 2.95 m, This machine is well-suited for this purpose and can serve as an effective solution for harvesting olives in an olive interspaced APV configuration.

Fig. 2. Modeling of an Agrivoltaic system with olive trees using Bifacial Radiance Raytracing Tool. Scene created to obtain the incident radiation in different points.
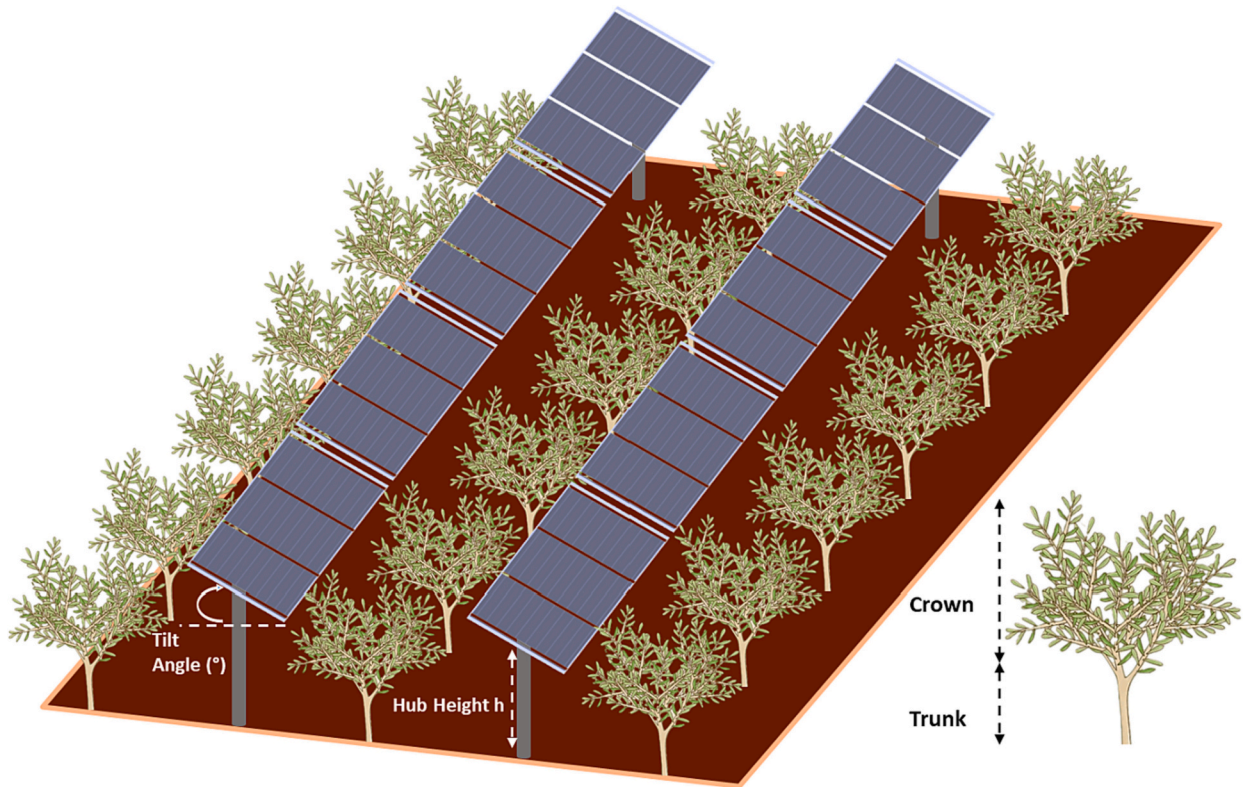
Fig. 3. Fixed-Tilt Interspaced Agrivoltaic: Schematic Diagram of Olive Tree Farming with PV Solar Panels.

2.2. APV dual model

2.2.1. Photovoltaic model

The PV power per unit active area in W/m^2 is calculated by following a standard procedure based on the following expressions [40,41]:

$$P_{PV} = G_{eff} * \eta_{STC} * AOIF * BSF * TF \quad (1)$$

$$G_{eff} = G_{front} + \varphi * G_{rear} \quad (2)$$

where G_{front} and G_{rear} represent the front and rear irradiance, respectively, on both sides of the bifacial PV module (bPV) in W/m^2, and G_{eff} denotes the bifacial effective irradiance in W/m^2, calculated as the sum of the front and the rear irradiance corrected by the bifaciality factor (φ), which was considered to be 70%. η_{STC} represents the PV module efficiency under Standard Test Conditions (STC, 1000 W/m^2, AM1.5G spectrum and 25 °C), which is considered to be equal to 20%. AOIF is the angle of incidence factor, which corrects the PV power when the sunrays do not fall perpendicularly on the module surface. It is assumed that the effect of the AOI is the same on both the front and rear sides of the module. The impact has been quantified by using the "iam. physical" model from PVLIB library [42]. BSF is the bifacial spectral factor that spectrally corrects the PV power [43]. *TF* is the thermal factor that performs the temperature correction. The four factors are dimensionless.

The BSF is calculated as:

$$BSF = \frac{G_{front} \bullet SF_{front} + \varphi_{Pmax} \bullet G_{rear} \bullet MM \bullet SF_{rear}}{G_{front} + \varphi_{P_{max}} \bullet G_{rear}} \quad (3)$$

$$SF_{front} = \frac{\int SR_{front}(\lambda) \cdot E_{front}(\lambda) \cdot d\lambda}{\int SR_{front}(\lambda) \cdot E_{front,ref}(\lambda) \cdot d\lambda} \cdot \frac{G_{front,ref}}{G_{front}} \quad (4)$$

$$SF_{rear} = \frac{\int SR_{rear}(\lambda) \cdot E_{rear}(\lambda) \cdot d\lambda}{\int SR_{rear}(\lambda) \cdot E_{rear,ref}(\lambda) \cdot d\lambda} \cdot \frac{G_{rear,ref}}{G_{rear}} \quad (5)$$

$$MM = \frac{\int SR_{rear}(\lambda) \cdot E_{rear,ref}(\lambda) \cdot d\lambda}{\int SR_{rear}(\lambda) \cdot E_{front,ref}(\lambda) \cdot d\lambda} \cdot \frac{G_{front,ref}}{G_{rear,ref}} \quad (6)$$

where SF_{front} and SF_{rear} are the front and rear spectral factors that quantify the influence of the incident spectrum on the front and rear sides of the PV module, respectively. *MM* is the mismatch factor between the two reference spectra (rear and front). $E_{front}(\lambda)$ and $E_{rear}(\lambda)$ represent the incident global spectral distribution on the front and rear sides of the bifacial module. This global spectrum is generated using the SMARTS tool and then scaled with the front and rear broadband irradiances obtained from Radiance simulations. $SR_{front}(\lambda)$ and $SR_{rear}(\lambda)$ are the front and rear spectral responses of the c-Si bifacial PV module [44]. $E_{front,ref}(\lambda)$ and $E_{rear,ref}(\lambda)$ are the reference spectra considered for the front and rear sides. These responses were obtained by averaging the measured spectral response curves from the front and rear sides of six commercially available bifacial PV modules. G_{front} and G_{rear} are the broadband global irradiance values on the front and rear sides, and $G_{front,ref}$ and $G_{rear,ref}$ are the front and rear broadband reference irradiances. Furthermore, all spectral factors were simulated using the same time step as the TMY dataset.

The TF is calculated by using the PV cell temperature and the thermal coefficient of the PV module as:

$$TF = 1 + \gamma \cdot (T_{cell} - T_{cell,STC}) \quad (7)$$

$$T_{cell} = T_a + \frac{T_{NOCT} - 20°C}{800W/m^2} \times (G_{front} + G_{rear}) \quad (8)$$

where T_{cell} is the cell temperature and $T_{cell,STC}$ is the cell temperature under STC and equals to 25 °C. The T_{cell} is determined by using the ambient temperature T_a data obtained from the TMY dataset, in combination with the global irradiance of the PV module. The global irradiance is calculated as the sum of the front and rear irradiances, applying the method described in the IEC 61853–1 standard and based

on the Nominal Operating Cell Temperature (NOCT). For the PV module used in this study, the NOCT is 42 °C and γ is equal to -0.0036 °C. An integral of the power P_{PV} over the time period of interest is performed to determine the energy produced by the PV system in kWh/m^2. In this study, potential losses, including soiling, electrical mismatch, wire heating, and DC/AC conversion, among others, have not been considered, even though they have the potential to reduce the PV yield. This choice is rooted in the observation that these additional losses tend to remain relatively constant and do not vary based on the APV system's configuration or operational conditions.

2.2.2. Olive tree crop model

The olive tree development depends on the incident spectral irradiance and its spectral absorption. To calculate the incident spectrum on the olive tree, $E_{plant}(\lambda)$ in $(W/m^2.nm)$, a two-step process is followed. First, the TMY data obtained from PVGIS serves as the primary irradiance input for the Bifacial Radiance Tool. Within this framework, the TMY data provides hourly listings of both direct and diffuse irradiances. The BR Tool subsequently conducts Ray tracing simulations with the same time step, aided by sensors strategically placed on the olive trees. These simulations enable the calculation of the broadband irradiance intercepted by the trees. Second, to determine the spectral irradiance received by the olive trees, the SMARTS tool is employed. This tool generates the spectral profile of the global irradiance under given conditions. Subsequently, this simulated spectral global irradiance is scaled using the broadband irradiance data obtained from the Bifacial Radiance tool. The resulting spectral data offers a highly accurate representation of the incident irradiance on the olive tree, capturing the specific wavelengths and their corresponding intensities in a comprehensive manner. This combined approach ensures that the incident spectrum on the olive tree is appropriately characterized in terms of both broadband and spectral components.

The scaling was done as:

$$E_{\text{plant}}(\lambda) = \frac{G}{\int GHI(\lambda)d\lambda} * GHI(\lambda) \tag{9}$$

where G in W/m^2 is the broadband global irradiance received by the olive tree from the raytracing simulation, $GHI(\lambda)$ in $W/m^2.nm$ is the spectral global irradiance from SMARTS simulated at the same sun position. Fig. 4 shows an example of a comparison between the spectra obtained from the SMARTS model and the spectra derived after the
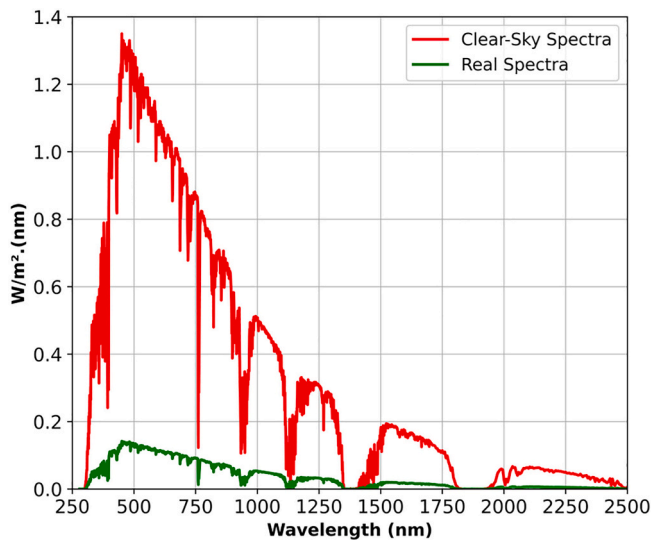

Fig. 4. A comparison between the spectrum obtained from SMARTS (Clear-sky Spectrum) and the scaled spectrum (Real Spectrum) on the 21st day of Mars at 10:00 AM with G = 596 W/m².

scaling process.

To evaluate the performance of the olive tree, the CO_2 absorbed by the photosynthesis in $mol\ (CO_2)/m^2$ is considered as the output of the olive tree model. It can be obtained by integrating the instantaneous PSN in $\mu mol\ (CO_2)/(m^2.s)$ over time. The PSN depends on the photosynthetic photon flux density (PPFD). This relation is a characteristic function for each crop. From the incident spectrum on the olive tree in $W/(m^2 \bullet nm)$, the PPFD is calculated in $\mu mol/m^2 \bullet s$, according to the next expression [45]:

$$PPFD_{\text{plant}} = \int_{400}^{700} \frac{E_{\text{plant}}(\lambda) \cdot \lambda}{N_A \cdot h \cdot c} \cdot d\lambda \tag{10}$$

where N_A is the Avogadro's number, h is the Planck's constant and c is the light velocity.

In this study, an analysis was conducted on three distinct olive varieties: Picual, Manzanilla, and Chemlali. These particular cultivars were chosen due to their wide availability and prevalence in specific regions. Picual olives are predominantly found in the Spanish province of Jaén, Spain [46]. Manzanilla olives, on the other hand, are endemic to Seville in Spain [47]. Lastly, Chemlali olives can be found in various Mediterranean countries, particularly Tunisia [48]. Moreover, we chose them because they exhibit different light responses. To accurately measure the photosynthetic light-response curves of these trees, a Licor LI-6800 portable photosynthetic system was used. This device is widely recognized and used for characterizing the light response of various crops [49,50]. It incorporates an automatic control mechanism that adjusts the concentration of CO_2 in the air stream.

By utilizing the Licor LI-6800 system, the response of gross carbon assimilation to absorbed light was assessed, which serves as a reliable indicator of the quantum efficiency of photosynthesis in olive tree leaves. Therefore, our analysis provides valuable insights into the photosynthetic performance of these trees. The experiment involved one-year-old plants cultivated within a controlled culture chamber, maintaining constant conditions of 40% humidity and a temperature of 21 °C. These plants adhered to a fixed daily light cycle of 16 h of light and 8 h of darkness. To enhance the reliability of the results, six plants of each type were employed, and measurements were repeated five times. The primary instrument for measurement was the LI-Cor 6800 photosynthetic analyzer. Before conducting measurements, the plants underwent a period of acclimatization to darkness the day prior. Subsequently, they were exposed to saturated pulsed light (3000 μmol $m^{-2}\ s^{-1}$, 300 ms duration) to determine both the minimum (F_0) and maximum (F_m) chlorophyll fluorescence levels. These values represent the status of the plant's photosystem II (PSII) reaction centers when they were fully closed (after dark acclimation) and fully open, respectively. Additionally, these fluorescence levels were measured when the plants were adapted to light (F_0' and F_m'). Utilizing this dataset, photosynthesis-light curves were constructed. Throughout these measurements, specific conditions were maintained within the analyzer, including a constant CO_2 concentration of 400 ppm, a relative humidity of 40%, an ambient temperature of 21 °C, a flow rate of 500 mmol/s, a fan speed of 10,000 rpm, and a light spectrum with specific color proportions (R90 B10). The light intensity varied in a gradient from 0 to 2000 $\mu mol\ m^{-2}\ s^{-1}$, with controlled waiting times between different light levels (ranging from 60 to 180 s). This gradient facilitated the precise modeling of the relationship between light intensity and the rate of net photosynthesis PSN in $\mu mol\ (CO2)/m^2s$. Fig. 5 presents the light responses of the three olive varieties.

The light source of the Licor LI-6800 unit used to characterize the different olive trees has a spectral distribution $E_{Licor}(\lambda)$, which differs from the incident spectrum on the trees. Thus, in order to improve the accuracy of the results, a spectral mismatch factor MM is considered. The mismatch can be obtained as:
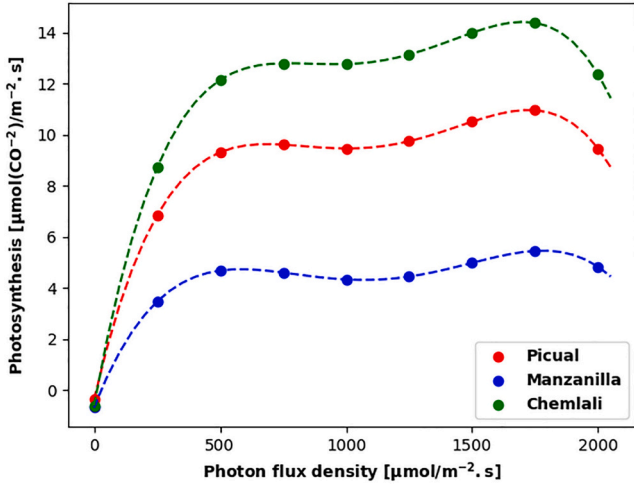
Fig. 5. Photosynthetic light response curves of three different olive tree varieties plotted against photosynthetic photon density.

$$MM = \frac{\int E_{\text{plant}}(\lambda) \cdot QY(\lambda) \cdot \lambda \cdot d\lambda}{\int E_{\text{Licor}}(\lambda) \cdot QY(\lambda) \cdot \lambda \cdot d\lambda} \cdot \frac{\int E_{\text{Licor}}(\lambda) \cdot \lambda \cdot d\lambda}{\int E_{\text{plant}}(\lambda) \cdot \lambda \cdot d\lambda} \tag{11}$$

where $QY(\lambda)$ represents the quantum yield of the tree. In this particular case, we have adopted the typical quantum yield proposed by McCree [51], which is recognized as being representative of various crops [51]. Additionally, the $E_{Licor}(\lambda)$ corresponds to a characteristic of the Licor LI-6800 light source, as illustrated in Fig. 6.

To accurately relate the PPFD emitted by the Licor to the $PPFD_{uncorrected}$ received by the plant, the following expression can be used:

$$PPFD = MM \cdot PPFD_{\text{uncorrected}} \tag{12}$$

PPFD refers to the amount of light available for photosynthesis, while PSN represents the rate at which plants convert that light energy into organic compounds through photosynthesis. Generally, until reaching a saturation point, the relationship between PPFD and PSN is positive, indicating that the higher the PPFD, the greater the PSN. Beyond the saturation point, further increases in PPFD may not significantly enhance photosynthesis and can even lead to a decrease in PSN due to factors such as photoinhibition. Photoinhibition occurs when the plant's photosynthetic apparatus becomes overwhelmed by an excess of light energy, leading to a reduction in the photosynthetic efficiency and to a potential damage to the plant [52]. However, this relationship is not linear and is influenced by several factors that affect the overall photosynthetic efficiency of a crop, including temperature, humidity and CO_2 concentration. In order to characterize this relationship, we employed a fitting process and determined that a fourth-order polynomial provides the best fit. This approach allowed us to accurately establish the relationship between the PPFD and the PSN for each olive cultivar as:

$$PSN = a_0 + a_1 \cdot PPFD + a_2 \cdot PPFD^2 + a_3 \cdot PPFD^3 + a_4 \cdot PPFD^4 \tag{13}$$

It is noteworthy that the photosynthetic rate PSN was modeled with high accuracy, as evidenced by an average coefficient of determination (R^2) value of 0.98. This outcome provides strong evidence supporting the quality of the crop photosynthesis PSN modeling conducted in this study. However, it is important to note that the light-response curves were measured under specific conditions of CO_2 content, temperature, and soil humidity. It is crucial to acknowledge that the light-response curves of crops can vary significantly based on these parameters. In this study, we assume that the light-response curves remain unchanged, considering the specified conditions. The integration of the instantaneous PSN over the relevant time interval enables the quantification of the CO_2 absorbed by photosynthesis in mol $(CO_2)/m^2$, which represents the primary output of the crop model. Since the critical periods affecting olive tree yield due to radiation are not clearly defined [53], this study
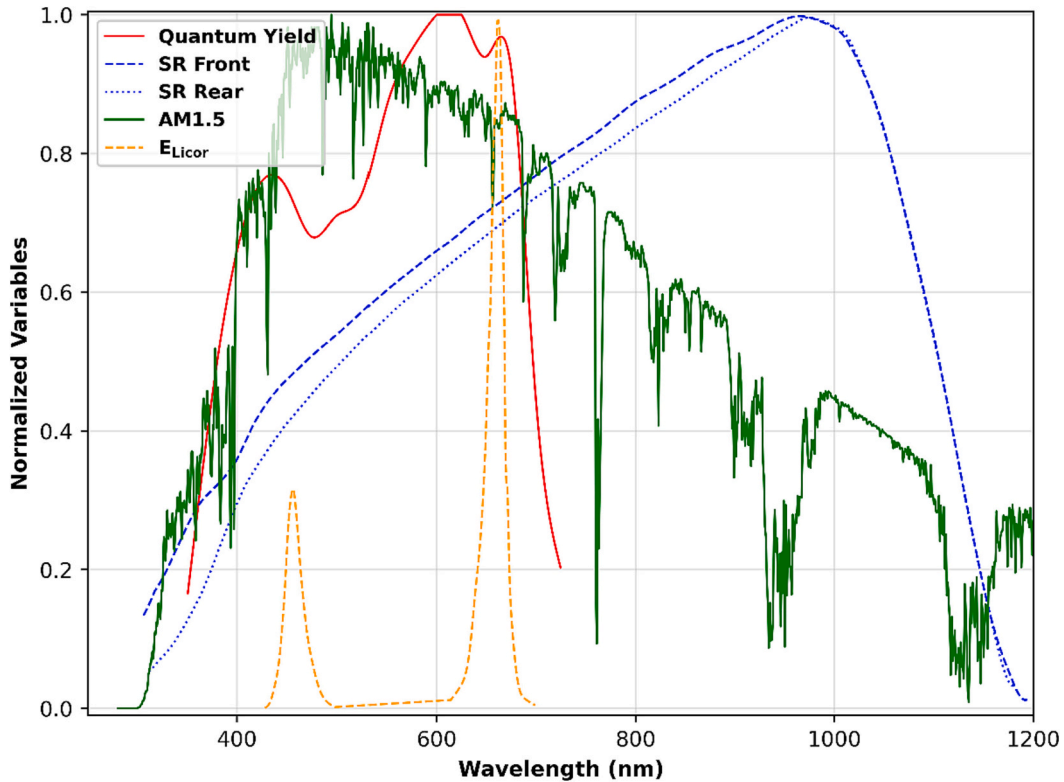

Fig. 6. *Standard ASTM G173–03 global spectrum, typical quantum yield (QY) of crops, as proposed by McCree* [51], $E_{Licor}(\lambda)$ *spectrum, and front and rear side spectral response of c-Si bifacial module.*

performs an annual calculation of olive yield to account for the uncertainty of when these critical periods occur throughout the year.

2.2.3. Measuring the benefits of APV: Land equivalent ratio

To evaluate the efficiency and productivity of an APV system, the Land Equivalent Ratio (LER) is a commonly used performance indicator [12]. LER quantifies the land productivity of the combined energy and crop outputs of an APV system compared to the productivity of stand-alone PV and crop systems, both using the same land area. The LER can be expressed as follows:

$$\text{LER} = \frac{Y_{\text{crop,APV}}}{Y_{\text{crop,ref}}} + \frac{Y_{PV,\text{APV}}}{Y_{PV,\text{ref}}} \quad (14)$$

where $Y_{PV,APV}$ is the energy yield for the APV and $Y_{PV,\text{ref}}$ is the energy yield of a reference traditional PV farm. $Y_{crop,APV}$ is the yield of olive trees grown in an APV system, and $Y_{crop,ref}$ represents the yield of reference super-intensive olive trees grown in an open field with a tree row spacing of 3.5 m and a tree height of 2.5 m. The reference PV farm under consideration is a fixed-tilt PV system without an APV configuration. It features PV modules tilted at 30°, a pitch of 3.5 m, a hub height of 3.5 m, and a ground albedo of light soil, with a broadband value of 0.25. No tracking system was considered in the reference PV farm to prevent an increase in PV yield. This ensures that any variation in yield ratio is solely attributed to the APV configuration and that it not a result of the inherent advantages of tracking systems. The number of sensors placed on PV modules and on the trees is kept the same in both the APV and reference configurations, simplifying the impact of the number of sensors under consideration. A LER value >1 indicates that the combined yield on the same land is higher than the yield of each system when implemented separately on the same land area.

2.2.4. Simplified approach for olive yield prediction

In this study, we have employed an approach to determine the olive yield in an agrivoltaic system. Our approach considers several key factors, including the spatial variation of sun irradiance, the spectral variation of sunlight, and the configuration of the APV system. Additionally, we consider the photosynthetic light response of the olive varieties to account for the variation in olive response at different PPFD values. Another approach to estimate crop yield, as suggested by Riaz et al. [54], utilizes a linear and quadratic model based on the light shading ratio R_{GR}. The shading ratio R_{GR} is defined as the ratio of the annual irradiance received by the crop in an APV configuration to the annual irradiance received by the same crop in an open field with no PV panels shading the crop.

The authors express the linear relationship as follows:

$$\frac{Y_{\text{crop,APV}}}{Y_{\text{crop,ref}}} = m*R_{GR} + (1-m) \quad (15)$$

where (m) represents the linear slope and signifies the sensitivity of the crop to shading, taking values between 0 and 1. In the ideal scenario where m equals 0, the shade has no effect on the crop. This method simplifies the calculation by reducing the dependency of crop yield on sunlight to solely the shading ratio, which can be easily determined using various commercial software packages, such as PVsyst [55] and SAM [56]. However, knowledge of the crop sensitivity is essential for accurate crop yield calculations. In a previous study [18], the same model was employed to estimate the yield of Arbequina olive trees under different shading conditions. The study considered the linear model with three levels of sensitivity: m = 0 (indicating no sensitivity to shading), m = 0.5 (average sensitivity to shading), and m = 1 (maximum sensitivity to shading). Nevertheless, precise determination of the sensitivity parameter m can significantly enhance the model's accuracy. In our study, we consider the determination of sensitivity for the three olive varieties and conduct a comparative analysis of the two approaches.

3. Results

An assessment of the performance of the APV system for different configurations of PV modules has been made. The energy production and the olive yield were computed based on the varying levels of shading cast on the trees, which were determined by the panel tilt angle and the hub height to the ground. The tilt angles of the PV panels considered ranged from 0 to 90°, while the hub height varied between 3 and 4.5 m with half-meter increments. The orientation of the panels was maintained towards the south.

3.1. Impact of the photovoltaic configuration on APV yields

In order to investigate the impact of the modules tilt and hub height on the PV annual energy and olive yields, these were normalized against reference cases: an open field bPV with a 30° tilt and a 3.5 m pitch for the PV yield, and an olive grove without PV for the olive yield. Typically, for monofacial PV modules in the northern hemisphere, the annual PV energy production reaches a maximum at a tilt close to the latitude of the location [57–59]. Similarly, for bifacial PV, the optimal tilt angle is often found to be equal to or slightly higher than the latitude [60,61]. This is the case for large values of the ground coverage ratio, which is defined as the ratio between the PV collector length and the row pitch [62]. However, it should be noted that for bifacial PV, the optimal tilt angle may be affected by surrounding albedo [63], as well as clearance, though the latter has a negligible effect for values >1 m [61].

The energy yield results of varying the bPV tilt angle are presented in Fig. 7 (left). The figure illustrates that the annual energy yield increases with an increase in the tilt angle from 0° to 30°. The maximum energy yield is achieved when the tilt angle is close to the Jaén latitude, which is 37.77°. However, as the tilt angle exceeds this value, the annual energy yield drops rapidly. When the tilt angle reaches 90°, the drop in the energy yield is 50%. The maximum PV yield ratio does not reach 1 for hub heights of 3 m and 4.5 m because it differs from the reference configuration at a height of 3.5 m. Furthermore, the reference case does not include olive trees, which means that all the irradiance received by the ground will be reflected to the rear side of the PV module, with a ground albedo. In the case of the APV, a portion of the reflected light from the ground is intercepted by the trees.

However, determining the optimal tilt angle is a tradeoff between maximizing the energy yield and ensuring adequate sunlight sharing between the PV panels and the olive trees. Fig. 7 (right) presents the annual olive yield for the three varieties of olive trees at a hub height of 4.5 m. The results show that the olive yield decreases with an increase in the bPV tilt angle. An increase in the PV tilt angle from 0° to 40° has resulted in a drop in the olive yield of about 1.48%, 1.76%, and 1.50% for Picual, Manzanilla, and Chemlali, respectively. The Manzanilla's yield decreases more when exposed to moderate light levels due to its relatively lower light saturation point. However, beyond this point, the olive yield rapidly increases to reach its maximum at 90° with a rise of 10.1%, 10.8%, and 10.7%, respectively.

The effect of height h on the energy yield of PV panels becomes noticeable when the height is lower than 1 m. This is because the intensity of light reflected on the rear side of the module increases with height. However, this effect becomes minimal above that height [64]. The results confirm this observation. For instance, a maximum variation in PV yield of 2.67% is observed between a height of 3 m and 4.5 m at a tilt of 90° (Fig. 7, Left). On the other hand, the olive yield is susceptible to shading caused by the PV modules. However, all three varieties show the same pattern of variation in olive yield with the PV module tilt and height. The annual average difference in olive yield between the three varieties is approximately 1.2%. Fig. 8 illustrates the variation in normalized annual Picual olive yield with the PV module tilt angle for different heights. The yield variation of three varieties of olive trees with hub height and PV tilt angle is listed in the annex.

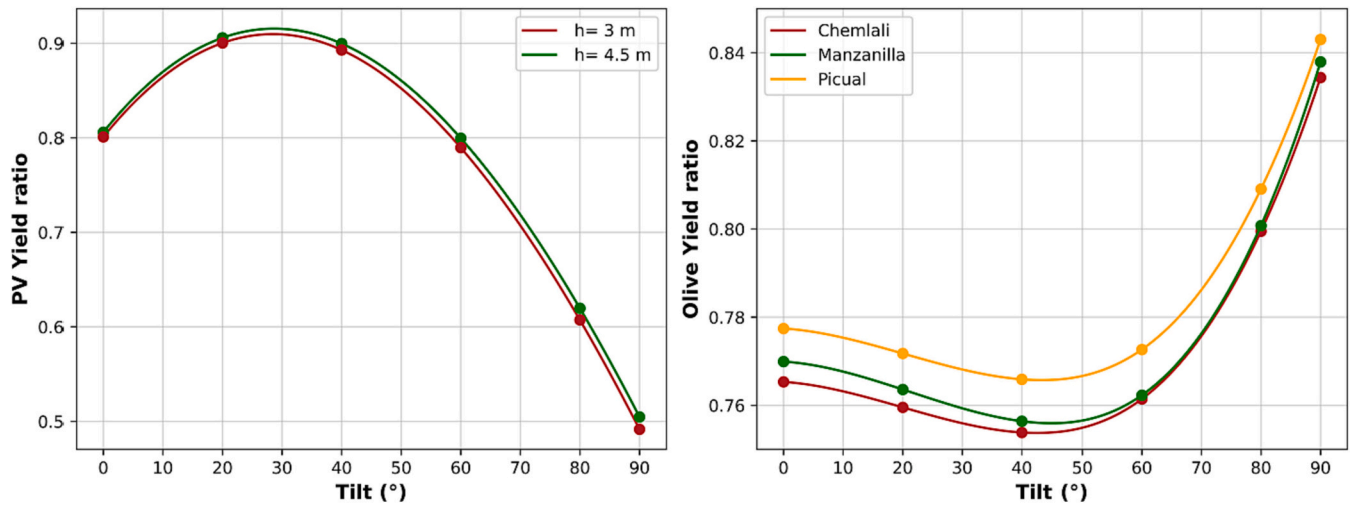The olive yield demonstrates an overall decrease in yield as the

Fig. 7. (Right) Yield response of three olive tree varieties to variations in PV module tilt angle. (Left) PV yield variation plotted against PV tilt angle at h = 3 m and 4.5 m.
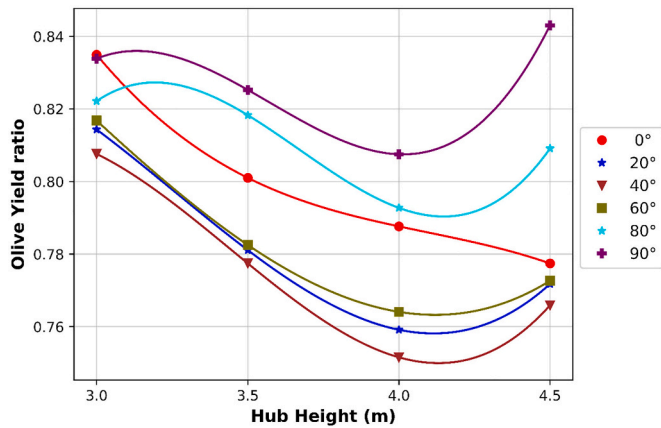

Fig. 8. Yield variation of Picual olive trees plotted against both hub height and PV tilt angle.

height of the PV modules increases in the horizontal configuration (tilt = 0°), resulting in a total decrease of 6.9%. This decline in olive yield is attributed to the increase in shading ratio, which rises as the height increases. In the inclined PV configuration (tilt >0°), there are two distinct cases to consider. The first case occurs when the tilt angle is <80°. In this scenario, as the hub height increases, the olive yield initially decreases until it reaches a minimum point between 4 and 4.5 m in height. However, beyond this minimum point, the yield starts to increase again. The second case pertains to tilt angles between 80° and 90°. In this situation, the yield shows a minimal increase with the height h, followed by a subsequent decrease until reaching a minimum between 4 and 4.5 m in height. After reaching this minimum point, the yield begins to increase once more. In the inclined PV configuration, as the PV panels are not directly positioned above the trees but rather in rows between the tree rows, increasing the PV hub height results in general in more shading on the olive trees. However, beyond a certain height threshold, the distance between the tree crowns and the PV modules becomes sufficient to allow irradiance to enter in between, reducing the shading ratio. This, in turn, leads to an increase in the olive yield.

3.2. Land equivalent ratio

The land equivalent ratio LER serves as a valuable metric to evaluate the combined influence of PV module tilt and hub height on PV and olive

yields. It can also offer insights into the land efficiency of an APV system that incorporates bifacial PV panels and olive tree cultivation. The LER exhibits a consistent pattern of variation across the three olive varieties, with an average difference of approximately 0.6% between them. Fig. 9 displays the variation of the LER with the tilt and hub height for the Picual variety. The results indicate that, across all configurations and for all three olive cultivars, the LER remains >1. This suggests that the combined yield on the same land is higher than what each system would produce individually if implemented separately on the same area. The LER gradually increases from a tilt of 0°, reaching its maximum increase in overall land productivity at around 71% when the tilt falls between 20 and 40°. This increase is primarily due to the increase in PV yield, which approaches the optimum tilt angle. However, beyond this point, the PV yield starts to decrease as the tilt angle increases, resulting in a decline in the LER. At a tilt of 90°, the LER reaches its minimum value, with a drop of 30%.

In contrast, when the height of the PV modules is increased from 3 m to 4 m, the LER decreases due to a corresponding decrease in the olive yield. However, when the PV module height reaches 4.5 m, the LER starts to increase again for all tilts except the horizontal tilt. This increase is observed because the shading level decreases with the increased height for these specific tilt angles. These findings suggest that at an optimum height, the optimization of PV yield is primarily determined by the module's tilt angle. Overall, the results of this analysis indicate that the variation in tilt angle has a greater impact on PV yield, while the variation in PV module height has a stronger effect on olive yield. This conclusion implies that finding the right balance between tilt angle and module height is crucial for maximizing the overall productivity of the land. Increasing the height of PV modules can indeed reduce shading on nearby trees. However, it is crucial to note that this improvement comes with a potential drawback: a significant increase in system costs, as highlighted in reference [65]. Therefore, optimizing an APV system involves a delicate balance between maximizing yields and minimizing economic expenditure. The ideal configuration may vary based on different perspectives, with some favoring higher profitability and others emphasizing lower initial costs.

3.3. Comparative analysis of olive yield models

To assess the sensitivity of olive trees to shading, a linear regression analysis was conducted. The analysis involved fitting the ratio of $Y_{crop,APV}/Y_{crop,ref}$ calculated with the olive model against the shading ratio, denoted as R_{GR} (as shown in Fig. 10). The shading levels of R_{GR} were determined based on the PV configuration considered in this
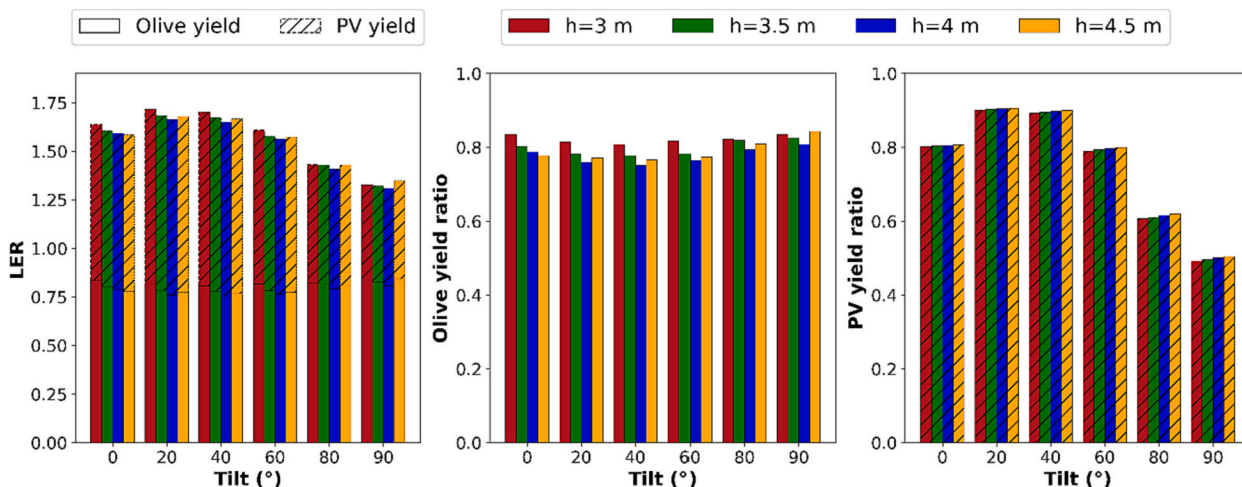
Fig. 9. Bar Plot of the Variation of Land Equivalent Ratio (LER), Olive Yield, and PV Yield of Picual Olive at Different PV Tilt Angles and Hub Heights.
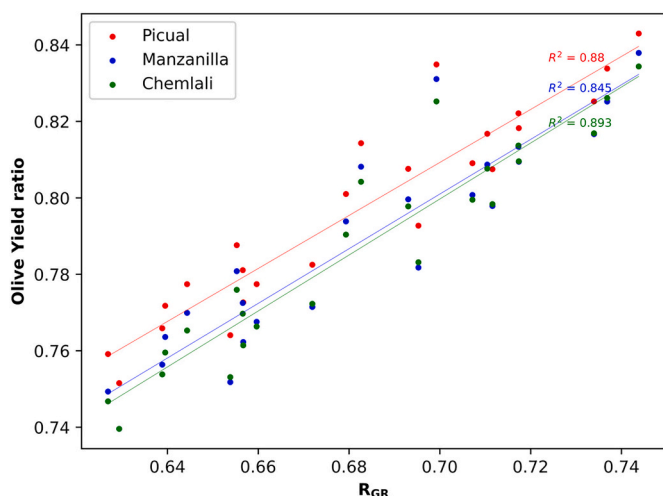

Fig. 10. Olive yield ratio from the olive model plotted against the shading ratio for three olive varieties, with the R^2 between olive yield ratio and shade ratio highlighted.

Fig. 11. Comparison of the simulated olive yield using two models.

study, which included tilt angles ranging from 0 to 90° and a hub height between 3 and 4.5 m. The resulting R_{GR} values ranged from 60% to 75%. The sensitivity values obtained for each variety of olive trees are presented in Table 1. The resulting sensitivity of the three olive tree varieties was found to be moderate, which explains the lower decrease in olive yield under APV system configurations.

To compare our olive model with the simplified linear model, we utilized the obtained sensitivity values m to calculate the ratio $Y_{crop,APV}/Y_{crop,ref}$ using the linear model. In Fig. 11, we present a comparison of the olive yield ratio results between the two models. To assess the accuracy of the simple model, we employed the coefficient of determination (R^2). Among the different olive varieties, the Chemlali variety demonstrated the highest accuracy, with an R^2 value of 0.893. It was closely followed by the Picual variety with $R^2 = 0.879$ and the Manzanilla variety with
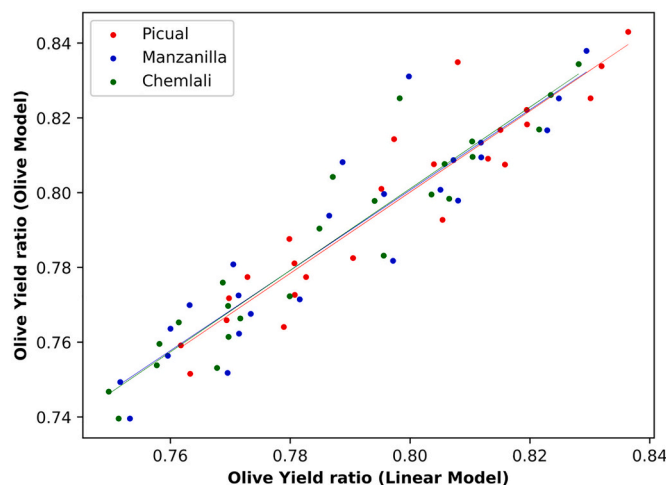
$R^2 = 0.845$. On the other hand, the linear model shows low values of errors compared to our model, with an average root mean square error (RMSE) value of 0.97% and an average mean bias error (MBE) of 0.73%. These low values indicate that the linear model can simplify the calculation of olive yield with high accuracy.

These results indicate a good correlation between the two methods. However, it is important to investigate other levels of shading, such as very low and very high shading ratios, to ensure that the correlation holds across all ranges. Additionally, this correlation was verified at an annual scale, but further investigations should explore lower time steps, such as daily and hourly, to capture more nuanced dynamics. Moreover, this comparison opens doors to studying additional types of crops on a global scale. Investigating different crops will allow us to generalize the findings and expand the applicability of our models. However, it is worth mentioning that these results can be further enhanced with experimental validation. Experimental validation will provide more robust evidence for the accuracy and reliability of our models. Furthermore, the APV system with olive orchard demonstrates promising yield results. However, to fully evaluate the feasibility and practicality of this system, an economic study is needed as future work. Assessing the profitability of the APV system will provide crucial insights for its implementation and adoption in real-world scenarios.

Table 1
Sensitivity to Shading of Three olive varieties in APV Systems.

Olive Variety	Sensitivity to shading, m
Picual	0.639
Manzanilla	0.666
Chemlali	0.671

4. Conclusions

In conclusion, this study offers significant insights into the performance of an APV system installed in southern Spain, particularly in relation to various bPV configurations. The findings demonstrate that the PV energy yield is maximized when the tilt angle closely aligns with the latitude, whereas a vertical inclination results in the lowest PV energy yield. Interestingly, the vertical inclination proves to be optimal for maximizing the yield of olive trees. The impact of varying the PV module height between 3 and 4.5 m is found to have minimal influence on the PV energy yield. When examining the inclined PV configuration, two distinct cases emerge. For tilt angles below 80°, the olive yield initially decreases with increasing hub height until reaching a minimum point between 4 and 4.5 m. Beyond this threshold, the yield begins to rise again. In the case of tilt angles between 80° and 90°, the yield experiences a slight increase with height, followed by a decline until reaching a minimum between 4 and 4.5 m. Subsequently, the yield starts to increase once more. Overall, the results indicate that the variation in tilt angle has a greater impact on the PV yield, while the variation in PV module height primarily affects the yield of olive trees. Additionally, the assessment of olive tree varieties reveals a moderate dependency on shading, making all varieties suitable candidates for APV applications.

Furthermore, a comparison between this model and a simplified linear model demonstrates a strong correlation between the two methods within the considered shading level. To summarize, this study provides valuable insights into the performance of APV systems and underscores the importance of considering optimal configurations to maximize both PV energy yield and olive tree yield. These findings can provide guidance for future agrivoltaic projects involving olive trees and contribute to the development of sustainable and efficient dual land use in agrivoltaic setups. However, experimental validation would be beneficial to verify the models using real crop yield data. Such validation would not only assess model accuracy but also underscore the potential utility of the study.

CRediT authorship contribution statement

Elmehdi Mouhib: Writing – original draft, Validation, Software, Methodology, Investigation, Data curation, Conceptualization. **Álvaro Fernández-Solas:** Writing – review & editing, Validation, Software, Methodology, Investigation, Data curation, Conceptualization. **Pedro J. Pérez-Higueras:** Writing – review & editing, Writing – original draft, Supervision, Methodology, Investigation. **Ana M. Fernández-Ocaña:** Validation, Investigation, Data curation. **Leonardo Micheli:** Writing – review & editing, Supervision, Methodology, Investigation. **Florencia Almonacid:** Writing – review & editing, Supervision, Methodology, Investigation, Conceptualization. **Eduardo F. Fernández:** Writing – review & editing, Supervision, Methodology, Investigation, Conceptualization.

Declaration of competing interest

The authors declare that they have no known competing financial interests or personal relationships that could have appeared to influence the work reported in this paper.

Data availability

Data will be made available on request.

Acknowledgements

Appendix A. Annexes

Table 2

Yield Variation of Chemlali, Manzanilla, and Picual Olive Trees with Hub Height and PV Tilt Angle.

		Tilt (°)					
	Height (m)	0	20	40	60	80	90
Chemlali	3.00	0.825	0.804	0.798	0.808	0.814	0.826
	3.50	0.790	0.770	0.766	0.772	0.810	0.817
	4.00	0.776	0.747	0.740	0.753	0.783	0.798
	4.50	0.765	0.760	0.754	0.761	0.799	0.834
Manzanilla	3.00	0.831	0.808	0.800	0.809	0.813	0.825
	3.50	0.794	0.773	0.768	0.771	0.809	0.817
	4.00	0.781	0.749	0.740	0.752	0.782	0.798
	4.50	0.770	0.764	0.756	0.762	0.801	0.838
Picual	3.00	0.835	0.814	0.808	0.817	0.822	0.834
	3.50	0.801	0.781	0.777	0.783	0.818	0.825
	4.00	0.788	0.759	0.752	0.764	0.793	0.807
	4.50	0.777	0.772	0.766	0.773	0.809	0.843

References

[1] Statista Research Department. Worldwide volume of food consumption 2015–2027. Statista. 2022. https://www.statista.com/forecasts/1298375/volume-food-consumption-worldwide#:~:text=The volume of global food,metric tons in that year (accessed May 25, 2023).

[2] Gorjian S, Bousi E, Özdemir ÖE, Trommsdorff M, Kumar NM, Anand A, et al. Progress and challenges of crop production and electricity generation in agrivoltaic systems using semi-transparent photovoltaic technology. Renew Sustain Energy Rev 2022;158:112126. https://doi.org/10.1016/j.rser.2022.112126.

[3] Dinesh H, Pearce JM. The potential of agrivoltaic systems. Renew Sustain Energy Rev 2016;54:299–308. https://doi.org/10.1016/j.rser.2015.10.024.

[4] Marrou H, Dufour L, Wery J. How does a shelter of solar panels influence water flows in a soil–crop system? Eur J Agron 2013;50:38–51. https://doi.org/10.1016/j.eja.2013.05.004.

[5] Uchanski M, Hickey T, Bousselot J, Barth KL. Characterization of agrivoltaic crop environment conditions using opaque and thin-film semi-transparent modules. Energies 2023;16:3012. https://doi.org/10.3390/en16073012.

[6] Hartzell S, Bartlett MS, Porporato A. Unified representation of the C3, C4, and CAM photosynthetic pathways with the Photo3 model. Ecol Model 2018;384:173–87. https://doi.org/10.1016/j.ecolmodel.2018.06.012.

[7] Yin X, Struik PC. C 3 and C 4 photosynthesis models: an overview from the perspective of crop modelling. NJAS Wageningen J Life Sci 2009;57:27–38. https://doi.org/10.1016/j.njas.2009.07.001.

[8] Mahendra S, Ogren WL, Widholm JM. Photosynthetic characteristics of several C3 and C4 plant species grown under different light intensities 1. Crop Sci 1974;14: 563–6. https://doi.org/10.2135/cropsci1974.0011183X001400040021x.

[9] Bongi G, Soldatini GF, Hubick KT. Mechanism of photosynthesis in olive tree (Olea europaea L.). Photosynthetica 1987;21:572–8.

[10] Ladux FJ, Trentacoste ER, Searles PS, Rousseaux MC. Light quality environment and photomorphological responses of young olive trees. Horticulturae 2021;7:369. https://doi.org/10.3390/horticulturae7100369.

[11] International Olive Council (IOC). World Catalogue of Olive Varieties 2000:360. https://theolivecentre.com/product/World-Catalogue-of-Olive-Varieties#:~:text=Some 850 million olive trees,8.7 million hectares of land. (accessed May 26, 2023).

[12] Dupraz C, Marrou H, Talbot G, Dufour L, Nogier A, Ferard Y. Combining solar photovoltaic panels and food crops for optimising land use: towards new agrivoltaic schemes. Renew Energy 2011;36:2725–32. https://doi.org/10.1016/j.renene.2011.03.005.

[13] Brisson N, Gary C, Justes E, Roche R, Mary B, Ripoche D, et al. An overview of the crop model stics. Eur J Agron 2003;18:309–32. https://doi.org/10.1016/S1161-0301(02)00110-7.

[14] Trommsdorff M, Kang J, Reise C, Schindele S, Bopp G, Ehmann A, et al. Combining food and energy production: design of an agrivoltaic system applied in arable and vegetable farming in Germany. Renew Sustain Energy Rev 2021;140:110694. https://doi.org/10.1016/j.rser.2020.110694.

[15] Fernández EF, Villar-Fernández A, Montes-Romero J, Ruiz-Torres L, Rodrigo PM, Manzaneda AJ, et al. Global energy assessment of the potential of photovoltaics for greenhouse farming. Appl Energy 2022;309:118474. https://doi.org/10.1016/j.apenergy.2021.118474.

[16] Juillion P, Lopez G, Fumey D, Lesniak V, Génard M, Vercambre G. Shading apple trees with an agrivoltaic system: impact on water relations, leaf morphophysiological characteristics and yield determinants. Sci Hortic (Amsterdam) 2022;306:111434. https://doi.org/10.1016/j.scienta.2022.111434.

[17] Jiang S, Tang D, Zhao L, Liang C, Cui N, Gong D, et al. Effects of different photovoltaic shading levels on kiwifruit growth, yield and water productivity under "agrivoltaic" system in Southwest China. Agric Water Manag 2022;269: 107675. https://doi.org/10.1016/j.agwat.2022.107675.

[18] Ciocia A, Enescu D, Amato A, Malgaroli G, Polacco R, Amico F, et al. Agrivoltaic system: a case study of PV production and olive cultivation in Southern Italy. In: 2022 57th Int Univ Power Eng Conf Big Data Smart Grids, UPEC 2022 - Proc; 2022. p. 1–6. https://doi.org/10.1109/UPEC55022.2022.9917595.

[19] Fernández-Solas Á, Fernández-Ocaña AM, Almonacid F, Fernández EF. Potential of agrivoltaics systems into olive groves in the Mediterranean region. Appl Energy 2023;352:121988. https://doi.org/10.1016/j.apenergy.2023.121988.

[20] Lo Bianco R, Proietti P, Regni L, Caruso T. Planting systems for modern olive growing: strengths and weaknesses. Agric 2021;11:494. https://doi.org/10.3390/agriculture11060494.

[21] Allalout A, Krichène D, Methenni K, Taamalli A, Oueslati I, Daoud D, et al. Characterization of virgin olive oil from super intensive Spanish and Greek varieties grown in northern Tunisia. Sci Hortic (Amsterdam) 2009;120:77–83. https://doi.org/10.1016/j.scienta.2008.10.006.

[22] Pérez-Ruiz M, Rallo P, Jiménez M, Garrido-Izard M, Suárez M, Casanova L, et al. Evaluation of over-the-row harvester damage in a super-high-density olive orchard using on-board sensing techniques. Sensors 2018;18:1242. https://doi.org/10.3390/s18041242.

[23] Mersi A. SUPER-INTENSIVE (high density) PLANTATIONS n.d. https://olivolio.net/superintensiva_en.html (accessed June 21, 2023).

[24] DeAndreis P. One-Third of Global Olive Oil Production Comes from Intensive Farming. Olive Oil Times; 2022. https://www.oliveoiltimes.com/production/one-third-of-global-olive-oil-production-comes-from-intensive-farming/112809 [accessed September 27, 2023].

[25] El olivar en seto controla el 36% del AOVE mundial. Accord to a Study by Agromillora. 2022. https://www.olimerca.com/noticiadet/el-olivar-en-seto-controla-el-36-del-aove-mundial/b84be72ca4ce1d048706ce3312bf2320 (accessed September 27, 2023).

[26] Hwang S, Lee H, Kang Y. Energy yield comparison between monofacial photovoltaic modules with monofacial and bifacial cells in a carport. Energy Rep 2023;9:3148–53. https://doi.org/10.1016/j.egyr.2023.02.011.

[27] Koch P. Where limits to growth are tangible: the olive sector in Jaén and its bioeconomic future. Sustain Sci 2022. https://doi.org/10.1007/s11625-022-01236-6.

[28] Huld T, Müller R, Gambardella A. A new solar radiation database for estimating PV performance in Europe and Africa. Sol Energy 2012;86:1803–15. https://doi.org/10.1016/j.solener.2012.03.006.

[29] Ayala Pelaez S, Deline C. Bifacial_radiance: a python package for modeling bifacial solar photovoltaic systems. J Open Source Softw 2020;5:1865. https://doi.org/10.21105/joss.01865.

[30] Pelaez SA, Deline C, MacAlpine SM, Marion B, Stein JS, Kostuk RK. Comparison of Bifacial Solar Irradiance model predictions with field validation. IEEE J Photovoltaics 2019;9:82–8. https://doi.org/10.1109/JPHOTOV.2018.2877000.

[31] Pelaez SA, Deline C, Greenberg P, Stein JS, Kostuk RK. Model and validation of single-Axis tracking with Bifacial PV. IEEE J Photovoltaics 2019;9:715–21. https://doi.org/10.1109/JPHOTOV.2019.2892872.

[32] IEA PVPS Task 13. Bifacial PV modules & systems Experience and Results from International Research and Pilot Applications. Reliab Perform Photovolt Syst 2021: 1–168.

[33] CORDOBA D. Ficha Técnica BOBCAT T770 n.d. https://demolicionescordoba.es/maquinaria/maquinaria-ligera-de-demolicion/ficha-tecnica-bobcat-t770/ (accessed May 3, 2023).

[34] Pellenc.com. La cosechadora arrastrada para una cosecha más rápida y eficaz de la aceituna. n.d. https://www.pellenc.com/es-es/nuestros-productos/arboricultura-frutal-y-olivicultura/olivicultura/cosechar/arrastrada-olives-line (accessed June 19, 2023).

[35] How important is the pruning of the olive grove?. 2021. https://blog.esao.es/en/how-important-is-the-pruning-of-the-olive-grove#:~:text=The olive grove in hedge, from 1 to 2 meters. (accessed September 27, 2023).

[36] Gomes L, Nobre T, Sousa A, Rei F, Guiomar N. Hyperspectral reflectance as a basis to discriminate olive varieties—A tool for sustainable crop management. Sustainability 2020;12:3059. https://doi.org/10.3390/su12073059.

[37] Solar L. LR4-60HBD 350 - 380M. https://solarshop.baywa-re.lu/core/media/media.nl?id=172589&c=6376560&h=sz4zIXjDuHhyGuue0iyqpUxxBzLYNo1fQ9H_U0BcllaUBRd9&_xt=.pdf; 2013.

[38] Sun X, Khan MR, Deline C, Alam MA. Optimization and performance of bifacial solar modules: A global perspective. Appl Energy 2018;212:1601–10. https://doi.org/10.1016/j.apenergy.2017.12.041.

[39] ALMONDS''LINE. Olive harvester machine CV5045 n.d. https://www.agriexpo.online/prod/pellenc/product-168153-13285.html.

[40] Fernández EF, Soria-Moya A, Almonacid F, Aguilera J. Comparative assessment of the spectral impact on the energy yield of high concentrator and conventional photovoltaic technology. Sol Energy Mater Sol Cells 2016;147:185–97. https://doi.org/10.1016/j.solmat.2015.12.003.

[41] Fernández EF, Talavera DL, Almonacid FM, Smestad GP. Investigating the impact of weather variables on the energy yield and cost of energy of grid-connected solar concentrator systems. Energy 2016;106:790–801. https://doi.org/10.1016/j.energy.2016.03.060.

[42] Holmgren F, Hansen W, Mikofski A. pvlib python: a python package for modeling solar energy systems. J Open Source Softw 2018;3:884. https://doi.org/10.21105/joss.00884.

[43] Mouhib E, Rodrigo PM, Micheli L, Fernández EF, Almonacid F. Quantifying the rear and front long-term spectral impact on bifacial photovoltaic modules. Sol Energy 2022;247:202–13. https://doi.org/10.1016/j.solener.2022.10.035.

[44] Gostein M, Marion B, Stueve B. Spectral effects in albedo and rearside irradiance measurement for bifacial performance estimation. In: 2020 47th IEEE Photovolt. Spec. Conf. IEEE; 2020. p. 0515–9. https://doi.org/10.1109/PVSC45281.2020.9300518.

[45] Wu B-S, Rufyikiri A-S, Orsat V, Lefsrud MG. Re-interpreting the photosynthetically action radiation (PAR) curve in plants. Plant Sci 2019;289:110272. https://doi.org/10.1016/j.plantsci.2019.110272.

[46] Beltrán G, del Rio C, Sánchez S, Martínez L. Influence of harvest date and crop yield on the fatty acid composition of virgin olive oils from Cv. Picual J Agric Food Chem 2004;52:3434–40. https://doi.org/10.1021/jf049894n.

[47] Morales-Sillero A, Fernández JE, Torres-Ruiz JM, Montero A. Influence of irrigation scheduling on fruit quality of young potted "Manzanilla De Sevilla" Olive trees. Acta Hortic 2011:177–82. https://doi.org/10.17660/ActaHortic.2011.888.19.

[48] Khlif M, Ayadi M, Grati-Kammoun N, Arous MN, Rekik H, Hamdi MT, et al. Identifying chemlali olive variety in its traditional area. Acta Hortic 2002:117–20. https://doi.org/10.17660/ActaHortic.2002.586.16.

[49] Lawrence EH, Stinziano JR, Hanson DT. Using the rapid A-C i response (RACiR) in the Li-Cor 6400 to measure developmental gradients of photosynthetic capacity in poplar. Plant Cell Environ 2019;42:740–50. https://doi.org/10.1111/pce.13436.

[50] Li T, Heuvelink E, Dueck TA, Janse J, Gort G, Marcelis LFM. Enhancement of crop photosynthesis by diffuse light: quantifying the contributing factors. Ann Bot 2014; 114:145–56. https://doi.org/10.1093/aob/mcu071.

[51] McCree KJ. The action spectrum, absorptance and quantum yield of photosynthesis in crop plants. Agric For Meteorol 1972;9:191–216. https://doi.org/10.1016/0002-1571(71)90022-7.

[52] Demmig-Adams B, Adams WW. PHOTOSYNTHESIS AND PARTITIONING | Photoinhibition. In: Encycl Appl Plant Sci. Elsevier; 2003. p. 707–14. https://doi.org/10.1016/B0-12-227050-9/00091-0.

[53] Lémole G, Weibel AM, Trentacoste ER. Effect of shading in different periods from flowering to maturity on the fatty acid and phenolic composition of olive oil (cv. Arbequina). Sci Hortic (Amsterdam) 2018;240:162–9. https://doi.org/10.1016/j.scienta.2018.06.005.

[54] Riaz MH, Imran H, Younas R, Butt NZ. The optimization of vertical bifacial photovoltaic farms for efficient agrivoltaic systems. Sol Energy 2021;230:1004–12. https://doi.org/10.1016/j.solener.2021.10.051.

[55] PVsyst. PVsyst – Logiciel Photovoltaïque. V 7211. https://www.pvsyst.com/; 2022.

[56] SAM. Home - System Advisor Model (SAM). Nrel. https://sam.nrel.gov/; 2020.

[57] Ullah A, Imran H, Maqsood Z, Butt NZ. Investigation of optimal tilt angles and effects of soiling on PV energy production in Pakistan. Renew Energy 2019;139: 830–43. https://doi.org/10.1016/j.renene.2019.02.114.

[58] Kaddoura Tarek O, Ramli Makbul AM, Al-Turki Yusuf A. On the estimation of the optimum tilt angle of PV panel in Saudi Arabia. Renew Sustain Energy Rev 2016; 65:626–34.

[59] Kacira M, Simsek M, Babur Y, Demirkol S. Determining optimum tilt angles and orientations of photovoltaic panels in Sanliurfa. Turkey Renew Energy 2004;29: 1265–75. https://doi.org/10.1016/j.renene.2003.12.014.

[60] Faiman D, Dolev A. Optimum orientation of bi-facial PV modules. 19th Eur Photovoltaics Sol Energy Conf 2004:2470–3.

[61] Asgharzadeh A, Marion B, Deline C, Hansen C, Stein JS, Toor F. A sensitivity study of the impact of installation parameters and system configuration on the Performance of Bifacial PV arrays. IEEE J Photovoltaics 2018;8:798–805. https://doi.org/10.1109/JPHOTOV.2018.2819676.

[62] Tonita EM, Russell ACJ, Valdivia CE, Hinzer K. Optimal ground coverage ratios for tracked, fixed-tilt, and vertical photovoltaic systems for latitudes up to 75°N. Sol Energy 2023;258:8–15. https://doi.org/10.1016/j.solener.2023.04.038.

[63] Yusufoglu UA, Lee TH, Pletzer TM, Halm A, Koduvelikulathu LJ, Comparotto C, et al. Simulation of energy production by bifacial modules with revision of ground reflection. Energy Procedia 2014;55:389–95. https://doi.org/10.1016/j.egypro.2014.08.111.

[64] Asgharzadeh A, Lubenow T, Sink J, Marion B, Deline C, Hansen C, et al. Analysis of the impact of installation parameters and system size on bifacial gain and energy yield of PV systems. In: 2017 IEEE 44th Photovolt. Spec. Conf. IEEE; 2017. p. 3333–8. https://doi.org/10.1109/PVSC.2017.8366690.

[65] Thomas SJ, Thomas S, Sahoo SS, G AK, Awad MM. Solar parks: A review on impacts, mitigation mechanism through agrivoltaics and techno-economic analysis. Energy Nexus 2023;11:100220. https://doi.org/10.1016/j.nexus.2023.100220.